ACS APPLIED MATERIALS & INTERFACES

Research Article

www.acsami.org

Iron Impurities as the Active Sites for Peroxidase-like Catalytic Reaction on Graphene and Its Derivatives

Ying Dong,[†] Jing Li,*[,†] Lei Shi,[†] and Zhiguang Guo*[,†,‡]

[†]State Key Laboratory of Solid Lubrication, Lanzhou Institute of Chemical Physics, Chinese Academy of Sciences, Lanzhou 730000, People's Republic of China

[‡]Ministry of Education Key Laboratory for the Green Preparation and Application of Functional Materials, Hubei University, Wuhan 430062, People's Republic of China

Supporting Information

ABSTRACT: We established four kinds of good dispersing systems of graphene and its derivatives with different structural characteristics to estimate their peroxidase-like activity. Besides graphene oxide (GO), it is demonstrated that defect-free graphene, low-oxygen graphene, and iron(III)-doped graphene oxide (GO-Fe) are all capable of H_2O_2 activation to oxidize peroxidase substrates. As for defect-free graphene, the dispersibility in reaction medium exerts great impact on its catalytic activity and our further judgements concerning the nature of active sites. Improved stability and further exfoliation of defect-free graphene in reaction medium are beneficial to the access of reactants to active sites on the basal planes and enhance its peroxidase-like activity, which is superior to that of low-oxygen graphene and much higher than that of GO. In addition, their peroxidase-like activity can be greatly inhibited by the addition of iron chelators. Interestingly, the introduction of trace ferric ions into GO does not lead to an apparent change except for remarkable increase of its peroxidase-like activity. Therefore, we propose that the observed iron impurities rather than the doped nonmetallic heteroatoms play an important role in the peroxidase-like activity of graphene and its derivatives. In this light, saturated iron(III) was immobilized onto the oxygen-donor coordination of GO to immensely promote its activity. The peroxidase-like activity of the prepared GO-Fe was systematically evaluated by using 3,3′,5,5′-tetramethylbenzidine and pyrogallol as peroxidase substrates and was compared to that of horseradish peroxidase and hemin. As a result, GO-Fe shows excellent peroxidase-like catalytic activity, which is comparable to that of hemin. Furthermore, GO-Fe was used for the quantitative detection of H_2O_2 and glucose.

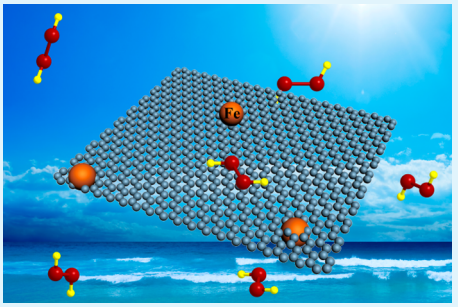

KEYWORDS: *defect-free graphene, low-oxygen graphene, graphene oxide, iron-doped graphene oxide, peroxidase-like activity*

1. INTRODUCTION

The mimics of natural enzymes with high catalytic activity and excellent substrate selectivity have attracted considerable interest. It is well-known that porphyrin derivatives (such as hemin) play an important role as the cofactors in the catalytic centers or the active sites of many natural enzymes, for example, redoxidase (such as peroxidase and catalase), oxygen carrier (such as hemoglobin and myoglobin), and electron transfer carrier (such as cytochromes). A large number of synthetically modified porphyrin models are being developed to provide the insights into structure−activity relationships and improve their catalytic activity or stability.[1−4] However, direct application of porphyrin derivatives as molecular catalysts is still of significant challenge due to the difficulty of catalyst recovery and the passivation of their catalytic activity. Hence, heterogenized molecular catalysts have become an alternative approach using specific supporters with high surface area including porous materials, natural clays, nanoparticles, and so on.[5−9]

Graphene, a one-atom-thick nanosheet of carbon densely arranged in a honeycomb crystal lattice, has triggered broad attention due to not only its outstanding physical properties, but also excellent chemical stability and high surface area (calculated value, 2630 $m^2\ g^{-1}$).[10−14] Therefore, graphene as a building block has been used to support horseradish peroxidase (HRP), hemoglobin, and iron porphyrin (such as hemin and FeTMPyP), forming recyclable and stable catalysts for H_2O_2 activation.[15−19] In addition, some metal and metal oxide nanomaterials (such as Fe_3O_4, Co_3O_4, gold nanoparticles, and nanoclusters) that were demonstrated for the peroxidase-like characteristics[20−23] have been also supported on graphene nanosheets acting as efficient catalysts for the peroxidase-like reactions.[24−27] These graphene nanosheets were obtained by oxidizing graphite to graphite oxide, followed by exfoliation and reduction to give single- and few-layered conductive products, because this method is cost-effective and suitable for large-scale production. Recently, a significant effort has been made to show the intrinsic (or "metal-free") peroxidase-like catalytic reaction on graphene oxide (GO), N-doped graphene, and other carbon nanomaterials (such as graphene nanomeshes,

Received: April 22, 2015
Accepted: June 26, 2015
Published: June 26, 2015

DOI: 10.1021/acsami.5b03486
ACS Appl. Mater. Interfaces 2015, 7, 15403−15413

carbon nanodots, single-walled and helical carbon nanotubes).[28−33]

As another point of view, there are some important reports suggesting that trace metallic impurities in carbon nanomaterials have a profound effect on their electrocatalytic activity.[34−37] In these works, onset potential, peak potential, and peak current density as important evidence are used to determine the active sites of carbon nanomaterials because these electrochemical signals are strongly dependent on the redox potential of selected molecular probes, and the interaction between the molecular probes and the active sites of carbon nanomaterials. However, other factors, such as chemical environments around active centers, electrode wetting properties, electrode surface structures, diffusion and adsorption of the selected molecular probes on the electrode surfaces, also have significant influence on the aforementioned electrochemical signals and could bring prominent disturbances on the judgements concerning the nature of active sites. What's more, carbon nanomaterials as heterogeneous catalysts have been utilized for facilitating a broad range of synthetic transformations.[38−40] Do metallic impurities in carbon nanomaterials act as active sites participating in liquid-phase catalytic reactions, including peroxidase-like catalytic reaction? Further determinations are needed as additional evidence to verify the possibility of metal mediated contributors. Here we established four kinds of good dispersing systems of graphene and its derivatives with different structural characteristics to estimate their peroxidase-like activity, and emphasized the important role of iron impurities in the peroxidase-like activity of graphene and its derivatives rather than their own characteristics. Moreover, saturated iron(III) was immobilized onto the oxygen-donor coordination of GO making use of the strong interaction between GO and ferric ions. This iron(III)-doped GO (GO-Fe) showed excellent catalytic activity and was explored as an effective biosensor platform for H_2O_2 and glucose.

2. EXPERIMENTAL SECTION

2.1. Materials. Graphite (natural, 325 mesh), 3,3′,5,5′-tetramethylbenzidine (TMB, 98%), pyrogallol (ACS, 99%), and hemin (98+ %) were purchased from Alfa Aesar. HRP (Type VI 274 units/mg solid), glucose oxidase (lyophilized powder, ∼200 U/mg), and polyvinylpyrrolidone (PVP, K30) were obtained from Sigma-Aldrich. TMB, pyrogallol, hemin, and HRP were stored in a refrigerator at 0−5 °C. Glucose oxidase was stored in a freeze space at about −20 °C. All other chemicals were of analytical grade and used as received without further purification.

2.2. Preparation of Defect-Free Graphene. Defect-free graphene was prepared according to the method reported by Coleman et al.[41,42] In a typical procedure, 0.5 g of graphite was dispersed in 100 mL of *N*-methyl-2-pyrrolidone (NMP) followed by a low-power sonication (Branson 1510E-MT) for 10 h. After sediment overnight (about 12 h), the top dispersion was carefully pipetted off and vacuum filtered through polyvinylidene fluoride membranes with 0.45 μm pores. Subsequently, the samples were washed by 100 mL of NMP and redispersed into 10 mL of NMP. Finally, well-dispersed graphene solution was obtained after centrifugation at 2000 rpm for 40 min.

2.3. Preparation of Low-Oxygen Graphene.[43] In a typical procedure, 1 g of graphite and 0.2 g of $KMnO_4$ were added into 100 mL of commercial $HClO_4$ (about 70%). This mixture was stirred for 2 h at 60 °C and then poured into 100 mL of water. Afterward, 10 mL of 30 wt % H_2O_2 was added to react with as-formed manganese oxides. The suspension was vacuum filtered through mixed cellulose ester membranes with 0.45 μm pores followed by washing with about 4 M HCl (three times) and abundant water. The product was redispersed in water (200 mL). The suspension was then sonicated for 1 h in the low-power sonic bath. After sediment overnight, the top dispersion was carefully pipetted off and vacuum filtered by using mixed cellulose ester membranes with 0.45 μm pores. Subsequently, the samples were redispersed into 10 mL of water. Finally, the good dispersion of low-oxygen graphene was obtained after centrifugation at 2000 rpm for 40 min.

2.4. Preparation of GO and GO-Fe. GO was synthesized by the modified Hummers method.[44,45] Natural graphite was oxidized by $NaNO_3$ and $KMnO_4$ in concentrated sulfuric acid. Solutions of 30% H_2O_2 and about 4 M HCl (three times) were used to remove as-formed manganese oxides and other metal ions as much as possible. After being washed with water, the precipitates were dispersed into water, which formed atomically thin GO by a low-power sonication. Next, the pH of GO aqueous solution was adjusted to 2 by 1 M HCl solution. In another flask, 1 M $FeCl_3$ was prepared by using 0.01 M HCl solution to avoid the hydrolyzation of ferric ions. Afterward, GO and $FeCl_3$ aqueous solutions were mixed under stirring for 24 h. The mixed solution was centrifuged at 9000 rpm followed by washing with abundant water (more than five times). Finally, GO-Fe was redispersed into water and stored for use.

In addition, a smaller amount of ferric ions was immobilized on the two-dimensional surface of GO. Twenty microliters of 0.1 M $FeCl_3$ in 0.01 M HCl solution was mixed with 20 mL of about 1 g/L GO aqueous solution under stirring for 24 h. The mixed solution was centrifuged at 9000 rpm after 1 M NaCl was added, followed by washing with 1 M NaCl aqueous solution (more than five times). The iron mass ratio in GO-Fe was about 0.56 wt %, being defined as GO-Fe(0.56). The sample was redispersed into 20 mL of water and stored for use.

2.5. Characterizations. Transmission electron microscopy (TEM) and scanning transmission electron microscopy (STEM) images were obtained by a transmission electron microscope (Tecnai G2 TF20, FEI) equipped with an energy-dispersive X-ray (EDX) attachment. The TEM samples were prepared by dropping the homogeneous dispersions on copper TEM grids that were coated with a thin amorphous carbon film and then dried at room temperature. The exfoliated GO-Fe and the thickness were characterized by atomic force microscopy (AFM, AIST-NT SmartSPM) measurements. The nanosheets were coated on freshly cleaved mica surface through a drop-casting method and then vacuum-dried at 60 °C. Graphene thin films were prepared by vacuum filtration of graphene dispersions in aqueous solution through porous alumina membranes (0.2 μm, Whatman). The thin films were used for the characterization of scanning electron microscopy (SEM) and Raman analysis. SEM imaging was performed on a field emission scanning electron microscope (JSM-6701F, JEOL). All Raman spectra were obtained on a Renishaw inVia Raman microscope with 632.8 nm wavelength laser light. X-ray photoelectron spectroscopy (XPS) analysis was carried out on a PHI-5702 X-ray photoelectron spectrometer. The thermal properties of samples were characterized by thermal gravimetric analysis (TGA, NETZSCH STA 449F3). The sample measurements were taken under a N_2 atmosphere from room temperature to 1000 at 10 °C min^{-1} for graphite and defect-free graphene, or in air at 5 °C min^{-1} for GO-Fe. All UV−vis absorption spectra were recorded by using a Cary 60 spectrophotometer (Agilent).

2.6. Kinetic Analysis. The concentrations of defect-free graphene and low-oxygen graphene were measured by UV−vis absorption spectroscopy. The absorption coefficients at 660 nm of defect-free graphene and low-oxygen graphene are 3620 and 3476 L g^{-1} m^{-1}, respectively.[42,43] The concentrations of the stored GO and GO-Fe were determined by a definite volume of their aqueous solution and the mass measurement of the precipitates by centrifugation and vacuum drying at 60 °C. Kinetic measurements were carried out in time course mode by monitoring the absorbance change at 652 nm for TMB and at 420 nm for pyrogallol on the UV−vis spectrophotometer. $A = A_t - A_0$, where A is the absorbance used to analyze the catalytic kinetic parameters, A_t is the absorbance along the reaction time, and A_0 is the absorbance of catalyst solution before catalytic reaction.

Before we tested the peroxidase-like activity of defect-free graphene, defect-free graphene dispersion was mixed with PVP aqueous solution

DOI: 10.1021/acsami.5b03486
ACS Appl. Mater. Interfaces 2015, 7, 15403−15413

at the same concentration followed by a low-power sonication for different time. The catalytic activity of graphene and its derivatives was measured in a reaction volume of 2 mL of buffer solution (25 mM NaAc buffer, pH = 3.5, at room temperature) with 0.8 mM TMB or 2 mM pyrogallol as a substrate, and H_2O_2 concentration was 5 mM for TMB or 50 mM for pyrogallol, unless otherwise stated. The Michaelis−Menten constant was calculated by using the Lineweaver−Burk plots of double reciprocal of the Michaelis−Menten equation:

$$1/\nu = (K_m/V_{max}) \times (1/[S]) + 1/V_{max}$$

Glucose detection was performed as follows: (1) 0.1 mL of 4 g/L glucose oxidase and 0.1 mL of glucose at different concentrations in 0.5 mM Na_2HPO_4 buffer (pH = 7.0) were mixed and incubated at 37 °C for 1 h; (2) 2 mL of 25 mM NaAc buffer (pH = 3.5), 0.05 mL of 32 mM TMB, and 0.05 mL of 0.8 g/L GO-Fe stock solutions were added into the above 0.2 mL glucose reaction solutions; (3) the mixed solutions in step 2 were incubated for 10 min at room temperature and then used for the measurements of 652 nm absorbance.

2.7. Electrocatalytic Activity of GO and GO-Fe in the Reduction of H_2O_2. Electrochemical measurements were performed on a CHI 660D apparatus. A three-electrode system including a platinum slice as an auxiliary electrode, a saturated calomel electrode as a reference electrode, and GO or GO-Fe coated on nickel foams as a working electrode was used for all electrochemical experiments. The experiments were carried out in a cell containing 0.1 M Na_2SO_4 (100 mL) at room temperature. The working electrodes were prepared by coating GO or GO-Fe onto the surface of nickel foams. Nickel foams (Changsha Lyrun New Material Co. Ltd., Changsha, China) were cleaned by 5 M HCl solution for 30 min to remove the NiO layer on the surface and then rinsed by water and ethanol. Nickel foams dried by N_2 purging were immersed in GO or GO-Fe aqueous solution. After sonication for 10 min, nickel foams containing GO or GO-Fe were vacuum-dried at 60 °C.

3. RESULTS AND DISCUSSION

Although the precise chemical structure of GO is still in considerable debate, GO as one of the most important graphene derivatives has attracted chemists' interests to explore its structure and chemical reactivity.[46] It is well-known that GO is easily reduced to electrically conductive products, demonstrating its high redox activity. This is mainly attributed to the inherent properties of some oxygen moieties (such as peroxy, epoxy, and aldehyde) of GO. It has been reasonably proposed that GO has the intrinsic peroxidase-like activity due to the electron transfer between GO and H_2O_2 bridged by these active oxygen moieties.[28] In addition, these oxygen-containing functional groups of GO also have strong coordination ability with transition metal ions. For example, there can be a strong interaction between salicylic acid-like structures of GO and ferric ions because the stability constant of Fe(III)-salicylic acid complex is up to 36.8. The strong interaction has been utilized to prepare graphene-based hydrogels.[47,48] Though strong acids are usually used to synthesize GO by employing both Hummers method and Staudenmaier method, trace iron impurities reserve in all probability. For example, the iron content was moderately decreased from 4224 to 927.6 ppm (Hummers method) using natural graphite as a starting material.[37] Therefore, we can reasonably assume that the peroxidase-like activity of GO and other graphene derivatives could be caused by the trace iron impurities.

To reveal the role of active oxygen moieties in the peroxidase-like catalytic reaction on graphene and its derivatives, we first prepared GO and defect-free graphene using natural graphite as a starting material (from a single source). GO was synthesized by a modified Hummers method.[44,45] At the same time, defect-free graphene was prepared according to the method reported by Coleman et al.[41,42] Natural graphite in NMP was exposed to a low-power sonication to achieve the minimum level of unnecessary oxygen defects. After the low-power sonication for 10 h, the exfoliated nanosheets are stabilized against aggregation by NMP due to the strong interaction between graphene nanosheets and the confined NMP molecules.[49] When the graphene NMP dispersion is added into water by a factor of 40:1 (water/NMP), the confined NMP molecules also stabilize graphene nanosheets in water, which provides the possibility to investigate the peroxidase-like activity of defect-free graphene.

Compared to GO with abundant oxygen-containing functional groups, defect-free graphene contains little oxygen content that was confirmed by various characterization techniques. The defect-free graphene aqueous dispersion was vacuum filtrated through porous alumina membranes (0.2 μm, Whatman) to form graphene thin films. Figure 1, panel a and

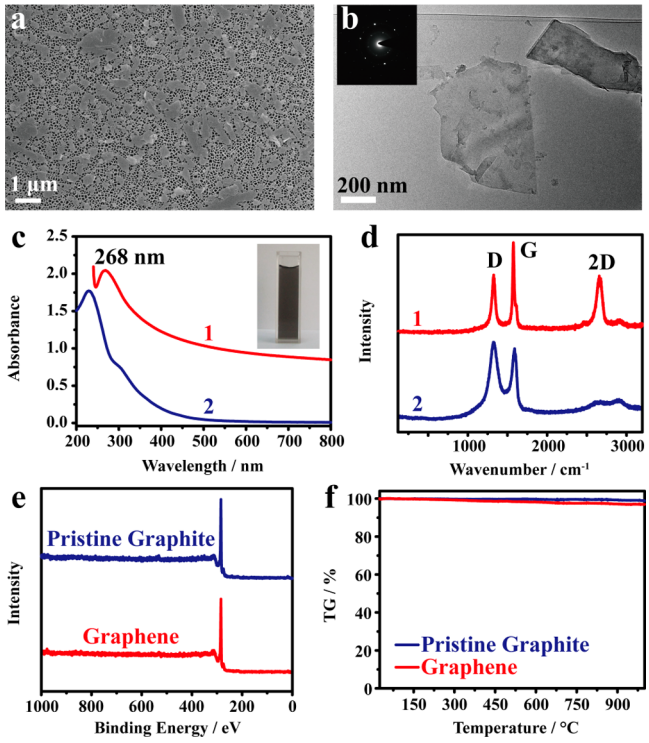

Figure 1. (a) SEM and (b) TEM images of defect-free graphene. The inset in panel b shows selected area electron diffraction pattern. (c) UV−vis absorption spectra of (1) defect-free graphene and (2) GO in aqueous solution. The inset shows the photograph of defect-free graphene in aqueous solution. (d) Raman spectra of (1) defect-free graphene and (2) GO. (e) XPS spectra of pristine graphite and defect-free graphene. (f) TGA of graphite and defect-free graphene.

Figure S1 of the Supporting Information show the photograph and SEM images of the graphene thin films. It is clearly seen that the uniform films consist of multilayered flakes with sizes of about 0.1−1 μm. A small quantity of the graphene dispersion was also dropped onto copper TEM grids. Figure 1, panel b exhibits a typical bright-field TEM image of the flakes. They are accordant to the flakes observed by SEM. The inset in Figure 1, panel b displays selected area electron diffraction pattern. The diffraction pattern of the graphene flakes shows the typical six-fold symmetry peaks, indicating the formation of defect-free graphene with high crystallinity. Notably, the {2110} spots

DOI: 10.1021/acsami.5b03486
ACS Appl. Mater. Interfaces 2015, 7, 15403−15413

appear to be more intense than the {1100} spots, corresponding to multilayers with AB stacking and incomplete exfoliation of the graphene flakes in water.[41] The STEM image further demonstrates the formation of the multilayered flakes (Figure S2a). In addition, EDX point analysis confirms the presence of trace iron impurities in the multilayered architecture and little oxygen content (Figure S2b).

The defect-free graphene aqueous dispersion stabilized by NMP molecules is suitable for the characterization of UV−vis absorption measurements. The UV−vis absorption spectrum of the graphene dispersion displays an absorbance maximum at 268 nm and the whole absorption in the visible region (Figure 1c). This is obviously distinct from that of GO with an absorbance maximum at 230 nm, indicating that π-conjugated structures of the prepared graphene are greatly retained. Figure 1, panel d presents the Raman spectra of the liquid-exfoliated graphene and GO. The D-to-G band intensity ratios of defect-free graphene and GO are 0.66 and 1.08, respectively, suggesting that the prepared graphene has larger size of the ordered crystallite graphitic domains than GO. The higher D-to-G ratio of GO is ascribed to the existence of abundant oxygen defects and hole defects from deep oxidation. In addition, the 2D peak intensity of defect-free graphene is also stronger than that of GO, further implying that the low-power sonication greatly reserves the integrated structures of the nonoxidized graphene and to a great extent avoids the introduction of oxygen deficiency.

Figure 1, panel e shows XPS survey spectra of graphite and defect-free graphene. Only C 1s peak is observed at about 284 eV, which is mainly assigned to C−C components (Figure S3). In contrast, GO obviously presents C 1s and O 1s peaks at about 284 and 533 eV, respectively (Figure S4). The C 1s peak of GO includes one main C−C and abundant C−O components. The results verify that defect-free graphene has very few active oxygen moieties embedded into the honeycomb crystal lattice. Furthermore, TGA was used to determine the amount of foreign species introduced to the pristine graphite. As shown in Figure 1, panel f, defect-free graphene and graphite display similar profiles of thermal decomposition. Compared to the pristine graphite, the increased weight loss under a N_2 atmosphere of defect-free graphene is mainly assigned to the doped species (especially oxygen atoms and solvent molecules). Hence, the amount of the introduced foreign species can be quantified by the weight loss of the prepared graphene and graphite at 1000 °C. This is about 1.9 wt %, further reflecting a very small amount of oxygen moieties in the prepared graphene.

Afterward, we made the comparison of the peroxidase-like activity between defect-free graphene and GO with different oxygen contents. The liquid exfoliated method for preparing defect-free graphene dispersions is potential to open up a way to liquid-phase chemistry. However, it is found that defect-free graphene is hard to be well dispersed in water or other common solvents after the addition of electrolytes or washing by water, which strongly influences the evaluation of its peroxidase-like activity. The prepared graphene in the mixed solvent of NaAc buffer solution (pH = 3.5) and NMP (1/40 v/v) cannot activate H_2O_2 to oxidize TMB due to the aggregation of graphene flakes. To effectively stabilize defect-free graphene in the reaction solution, the same amount of PVP was added into the buffer solution before the graphene NMP dispersion was added. In this way, defect-free graphene stabilized by PVP is capable of the catalytic oxidation of the peroxidase substrate TMB, resulting in the color change (Figure S5). In spite of little oxygen content, the peroxidase-like activity of defect-free graphene is equivalent to that of GO (Figure 2).

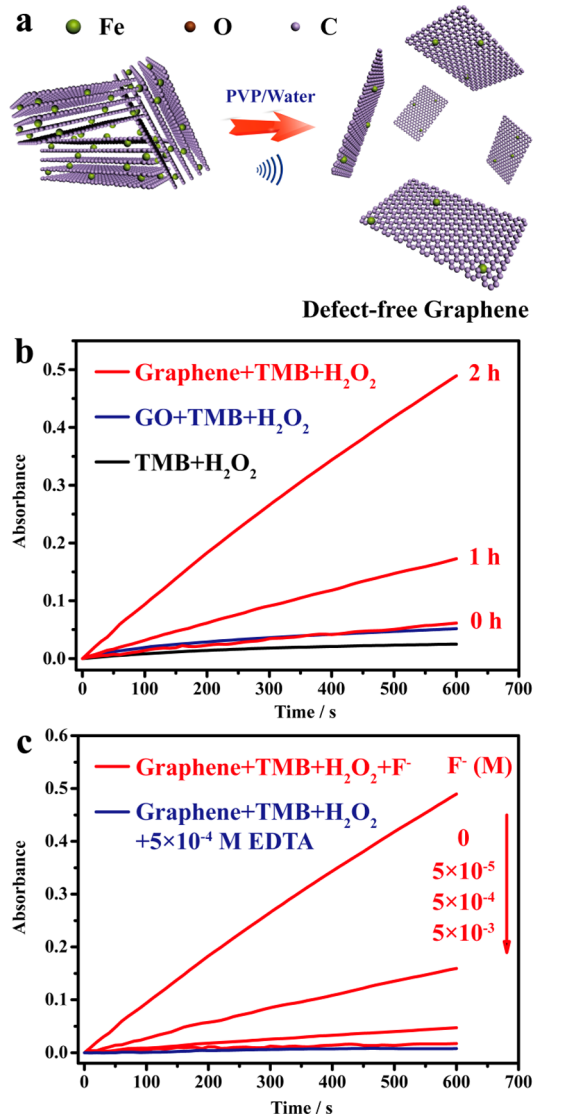

Figure 2. (a) Schematic for the further exfoliation of multilayered flakes favoring the access of reactants to the active sites on the basal planes of defect-free graphene. (b, c) Time-dependent absorbance changes at 652 nm of TMB catalyzed by 25 mg/L defect-free graphene and GO. Experimental conditions: 5 mM H_2O_2 and 0.8 mM TMB at room temperature, pH 3.5. (a) The catalytic activity of defect-free graphene after sonication for different time. (b) The catalytic activity of defect-free graphene before and after the addition of F^- and EDTA.

The defect-free graphene aqueous dispersion containing PVP was further treated by a low-power sonication. Interestingly, the peroxidase-like activity of defect-free graphene is dramatically increased with the sonication time and much higher than that of GO. Indeed, the low-power sonication cannot destroy the integrated structures of the prepared graphene, which is supported by the investigation of Raman analysis (Figure 3) but promotes further exfoliation of the multilayered flakes. This is beneficial to the access of reactants to the active sites on the basal planes of defect-free graphene, resulting in the acceleration of the color reaction (Figure 2a). Compared to GO, the enhanced peroxidase-like activity of defect-free

DOI: 10.1021/acsami.5b03486
ACS Appl. Mater. Interfaces 2015, 7, 15403−15413

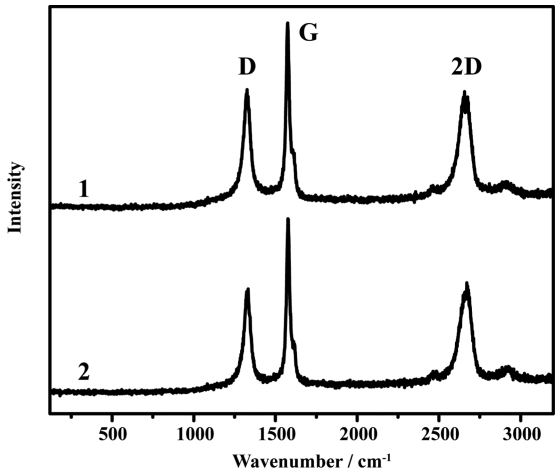

Figure 3. Raman spectra of defect-free graphene (1) before and (2) after a low-power sonication.

graphene is predominantly ascribed to higher iron content of defect-free graphene according to the results reported by M. Pumera and co-workers.[37]

What are the active sites? We propose two kinds of possible active sites on the basal planes of defect-free graphene. One is structural defects that are usually caused by the presence of nonhexagonal rings. The nonhexagonal rings possess a different electron cloud density from surrounded hexagonal rings and can interact with specific acceptor or donor molecules, which could favor the electron transfer between defect-free graphene and H_2O_2. The other one is the observed trace iron impurities. To address this question, we employed two kinds of complexing reagents without electrical activity to interfere with the peroxidase-like catalytic reaction such as fluorinion (F^-) and ethylene diamine tetraacetic acid (EDTA). As shown in Figure 2, panel b, the peroxidase-like activity of defect-free graphene is significantly decreased as F^- concentration is gradually increased. When F^- concentration is the same as H_2O_2 concentration (5 mM), H_2O_2 activation is drastically retarded. Here we suggest that the observed trace iron impurities rather than structural defects, and trace oxygen defects play a dominant role in the peroxidase-like catalytic reaction on defect-free graphene. The addition of F^- occupies the axial positions of the iron catalytic centers instead of H_2O_2 and gradually inhibits the oxidation of TMB. In the same way, only 0.5 mM EDTA can completely suppress the peroxidase-like activity of the prepared graphene due to stronger coordination ability of EDTA with iron active centers than that of F^-. Prospectively, the role of metallic impurities in the peroxidase-like activity of defect-free graphene could be equally important for its applications in the electrochemical sensors.[50−52]

In our previous work, low-oxygen graphene was synthesized under a simple reaction system of 5:1 graphite/$KMnO_4$ (generally 1:6 for Hummers' GO) in concentrated $HClO_4$.[43] We have revealed that low-oxygen graphene has an oxygen content of about 14 wt % from TGA and XPS measurements, which is more than that of defect-free graphene but much less than that of GO. Here, low-oxygen graphene as another representative graphene derivative was selected to further check the aforementioned viewpoint. The two-dimensional nanostructures of low-oxygen graphene are clearly observed by the TEM and STEM measurements (Figure 4a−d). Like defect-free graphene, the low-oxygen graphene aqueous dispersion also shows grayish−black instead of the typically brown−yellow GO solutions and also has an absorbance maximum at 268 nm and the absorption in the whole spectral region (Figure 4f). Distinctly, it has been demonstrated that without any dispersants and special solvent molecules, low-oxygen graphene can be well dispersed in most polar solvents including water at a wide range of pH (the inset in Figure 4f). Such advantage favors the study on the peroxidase-like activity of low-oxygen graphene. It is found that low-oxygen graphene shows lower peroxidase-like activity than defect-free graphene but much higher than GO. This result agrees with our suggestion that the peroxidase-like activity of graphene and its derivatives does not lie on their oxygen content. Note that weak signals on trace iron impurities can be also observed via an EDX analysis (Figure 4e). It is reasonable that the iron amount of low-oxygen graphene is lower than that of defect-free graphene due to the use of strong acid to fabricate low-oxygen graphene, very likely resulting in lower peroxidase-like activity. In addition, the peroxidase-like activity of low-oxygen graphene is also greatly retarded by the addition of F^- (Figure 5). The results confirm that low-oxygen graphene also contains trace iron impurities as catalytic centers to participate in the color reactions.

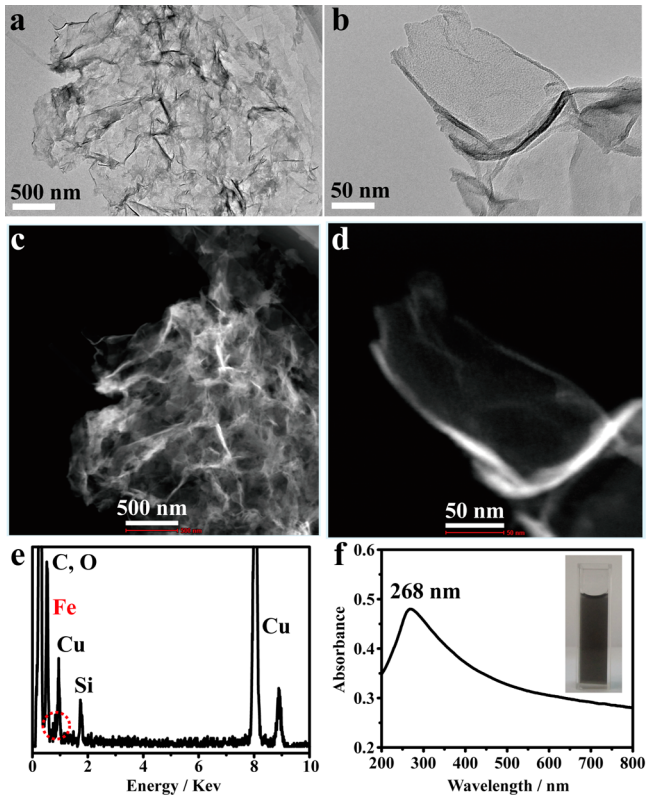

Figure 4. (a, b) TEM and (c, d) STEM images at different magnifications of low-oxygen graphene. (e) EDX profile of low-oxygen graphene. (f) UV−vis absorption spectrum of low-oxygen graphene in aqueous solution. The inset shows the photograph of low-oxygen graphene in aqueous solution.

Thus far, increasing interests for GO have been aroused due to its good dispersibility in various polar solvents and easy preparation by fully exfoliating graphite oxide. Next, we highlight that residual iron impurities play an extremely active role in the peroxidase-like catalytic reaction on GO. We mixed a very small amount of ferric ions with 1 g/L GO aqueous

DOI: 10.1021/acsami.5b03486
ACS Appl. Mater. Interfaces 2015, 7, 15403−15413

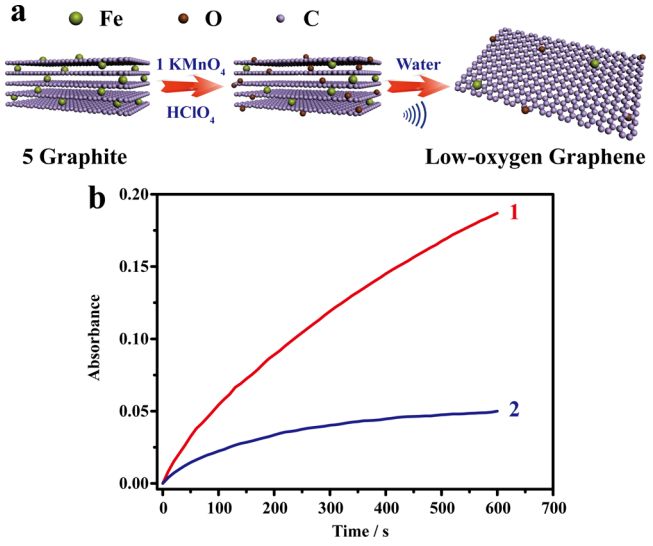

Figure 5. (a) Schematic for the preparation of low-oxygen graphene. (b) Time-dependent absorbance changes at 652 nm of TMB catalyzed by 25 mg/L low-oxygen graphene (1) before and (2) after the addition of 5 mM F^-. Experimental conditions: 5 mM H_2O_2 and 0.8 mM TMB at room temperature, pH 3.5.

solution under stirring for 24 h. If all ferric ions are fixed onto the two-dimensional surface of GO, the iron mass ratio in GO-Fe is about 0.56 wt %; therefore, we term the product as GO-Fe(0.56). Similar to GO, GO-Fe(0.56) is hard to be completely separated from the mixed solution by high-speed centrifugation. Hence, we added 1 M NaCl into the mixed solution to adequately separate the product under centrifugation at 9000 rpm. Subsequently, the product was washed by 1 M NaCl aqueous solution to remove the adsorbed free ferric ions. Compared to GO, it is found that GO-Fe(0.56) displays dramatically enhanced peroxidase-like activity due to the presence of more residual iron impurities (Figure 6c). Indeed, it is very difficult to observe any change after the introduction of trace iron impurities into GO any time. Even though abundant 1 M NaCl solution is used to wash GO-Fe(0.56), the iron impurities still persist in the two-dimensional nanostructures of GO. Otherwise, GO-Fe(0.56) and GO should perform equally in the peroxidase-like activity. The result strongly supports the viewpoints on the strong interaction between ferric ions and GO and indicates that trace levels of iron element in graphene and its derivatives are responsible for the so-called "metal-free" peroxidase-like catalysis.

We further mixed abundant ferric ions with GO in 0.01 M HCl solution to avoid the hydrolyzation of ferric ions. After being washed with abundant water, GO-Fe exhibits extremely efficient peroxidase-like activity at relatively low catalyst loadings (2 mg/L), as shown in Figure 6, panel d. The peroxidase-like activity of GO-Fe is superior to that of other graphene derivatives, such as defect-free graphene, low-oxygen graphene, and GO, owing to the highest iron content of GO-Fe. In addition, we compared the electrocatalytic behavior of GO and GO-Fe toward H_2O_2 reduction to further investigate the effect of iron impurities on their catalytic activity. GO and GO-Fe can be uniformly deposited on the surface of nickel foams (Figure 7). The porous architecture is advantageous to the diffusion of electrochemically active species on the electrode surfaces. In contrast to the poor response of the GO electrode, the GO-Fe electrode displays an enhanced

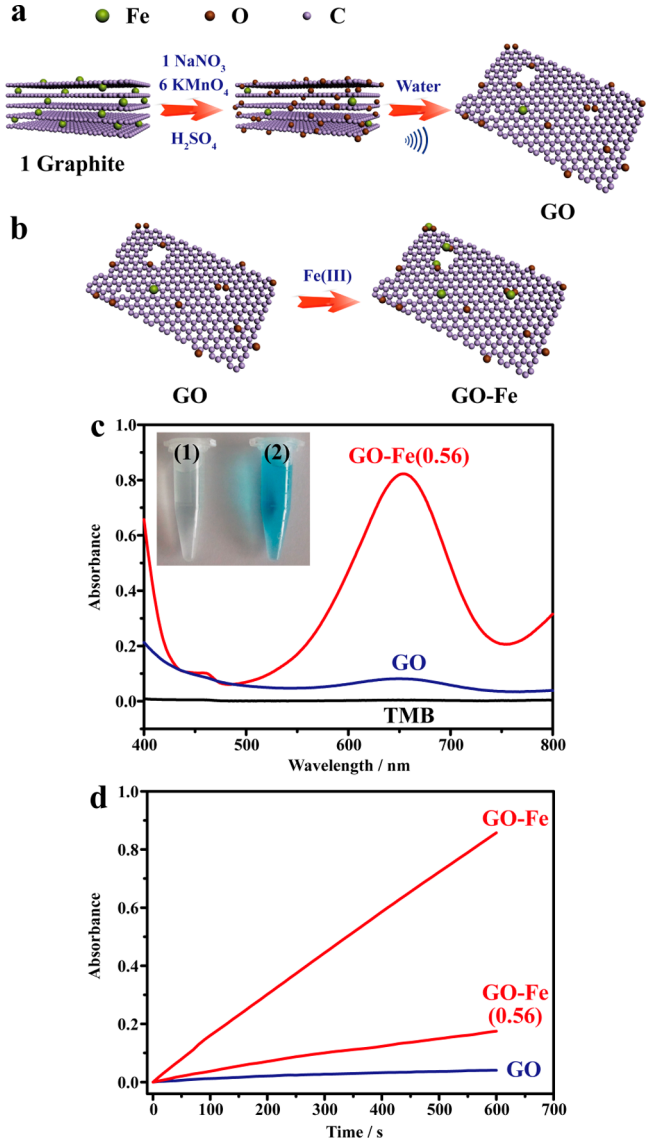

Figure 6. (a, b) Schematic for the preparation of GO and GO-Fe. (c) Typical UV−vis absorption spectra of TMB catalyzed by 25 mg/L GO and GO-Fe(0.56). The inset shows photographs of TMB catalyzed by (1) GO and (2) GO-Fe for 10 min. (d) Time-dependent absorbance changes at 652 nm of TMB catalyzed by 2 mg/L GO, GO-Fe(0.56), and GO-Fe. Experimental conditions: 5 mM H_2O_2 and 0.8 mM TMB at room temperature, pH 3.5.

current signal at −0.6 V. When H_2O_2 concentration is increased, the current signal on the GO-Fe electrode is increased, and the increasing amplitude is obviously higher than that on the GO electrode, implying a remarkable influence of iron impurities as active sites on the H_2O_2 activation of GO.

XPS and TGA were used to investigate the saturated amount of iron impurities immobilized onto the oxygen-donor coordination of GO. According to the XPS analysis of GO-Fe (Figure S6), C 1s and O 1s peaks are mainly observed at about 285 and 532 eV, respectively. The atomic ratio of carbon and oxygen is about 2.4, and iron atomic ratio in GO-Fe is about 1.3% (5.3 wt %). The existence of trivalent iron in GO-Fe is demonstrated by the Fe(III) $2p_{1/2}$ peak at 726.1 eV and the Fe(III) $2p_{3/2}$ peak at 712.8 eV. In addition, TGA was employed to further assess the iron atomic ratio in GO-Fe. Suppose C/O is 2.4, and only Fe_2O_3 (12 wt %) is produced after 1000 °C

DOI: 10.1021/acsami.5b03486
ACS Appl. Mater. Interfaces 2015, 7, 15403−15413

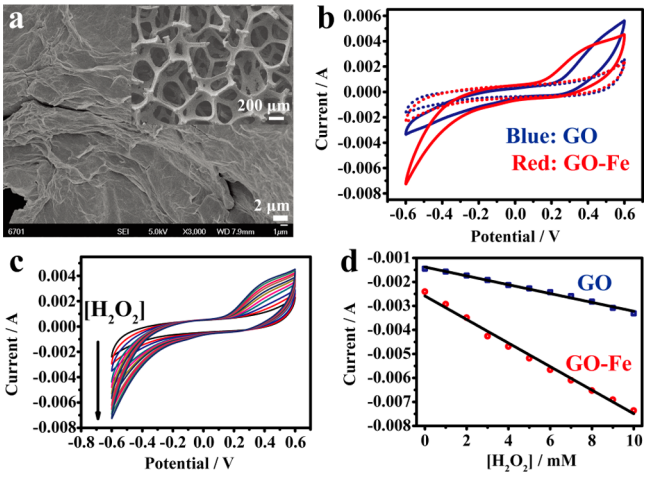

Figure 7. (a) SEM images at different magnifications of GO-Fe coated nickel foams. (b) Cyclic voltammograms recorded before (dot line) and after (solid line) addition of 10 mM H_2O_2 using GO and GO-Fe coated nickel foams as working electrodes. (c) Cyclic voltammograms recorded in the presence of different H_2O_2 concentrations using GO-Fe coated nickel foams as working electrodes. (d) Current density at −0.6 V versus H_2O_2 concentration using GO and GO-Fe coated nickel foams as working electrodes. Scan rate is 0.1 V/s.

thermal combustion of GO-Fe in air, about 2.1% (8.4 wt %) of iron atomic ratio in GO-Fe is obtained through calculation analysis (Figure S7). In this work, the calculation of iron atomic concentration in the catalytic systems was based on TGA data to estimate the peroxidase-like catalytic activity of GO-Fe.

Figure 8 shows typical TEM and STEM images at different magnifications of GO-Fe. GO-Fe exhibits typical two-dimensional nanosheets with a macroscopic wrinkling, which is commonly seen in TEM images of GO reported by the previous works.[47,48] The macroscopic wrinkling is mainly attributed to increased nanoscale corrugations induced by various oxygen-containing functional groups of GO and their coordination to ferric ions. Moreover, possible nanoparticles from the hydrolyzation of ferric ions are not obviously observed. The absence of possible nanoparticles on the two-dimensional surface of GO-Fe can be further confirmed by AFM investigation (Figure S8). Iron element can be detected on the smooth nanosheets via an EDX analysis (Figure 8d). Though the iron mass ratio in GO-Fe is up to 8.4 wt %, it is still difficult to clearly observe the presence of iron impurities, not to mention trace iron impurities of GO. From STEM images, it is clearly seen that GO-Fe is fully exfoliated. Importantly, the full exfoliation and good dispersibility of GO-Fe in aqueous solution make the active sites of iron catalytic centers all accessible. Therefore, it is proposed that GO-Fe as a potential peroxidase-like catalyst will be explored as an effective biosensor platform for H_2O_2 and glucose.

To utilize this discovery about the important role of iron impurities in the peroxidase-like activity of graphene and its derivatives, we systematically evaluated the peroxidase-like activity of GO-Fe using TMB and pyrogallol as peroxidase substrates and made comparison with HRP and hemin. It is observed that GO-Fe is capable of H_2O_2 activation to oxidize peroxidase substrates TMB and pyrogallol to produce a blue color and a yellow color, respectively. The catalytic rates of the peroxidase-like color reactions have a first-order dependence on the GO-Fe concentration (Figure 9). In the presence of excess TMB, GO-Fe exhibits high stability and steady catalytic

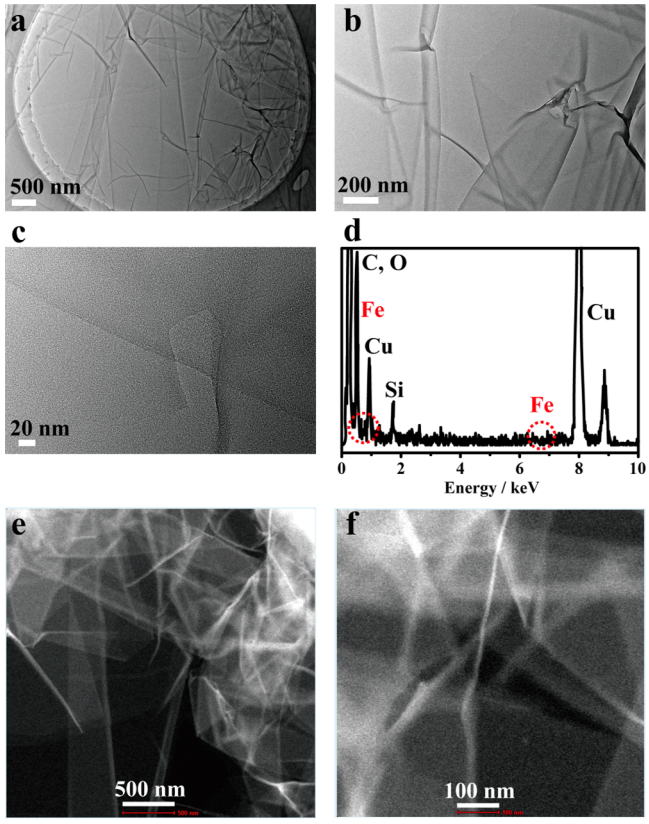

Figure 8. (a–c) TEM and (e, f) STEM images at different magnifications of GO-Fe. (d) EDX profile of GO-Fe.

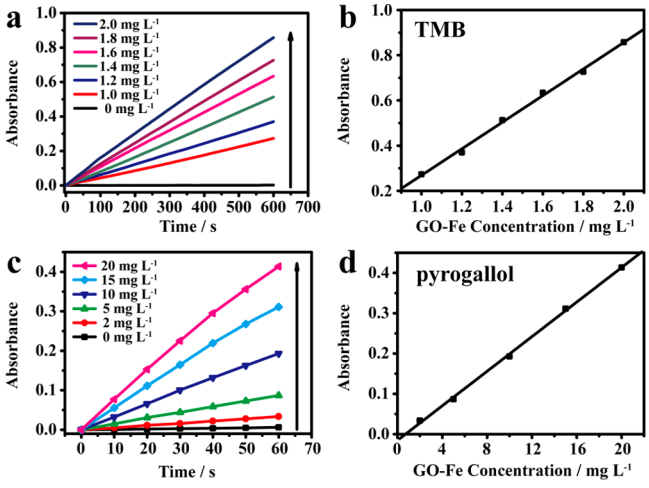

Figure 9. Time-dependent absorbance changes at (a) 652 nm of TMB and (c) 420 nm of pyrogallol catalyzed by GO-Fe at different concentrations. (b) The absorbance at 652 nm of TMB after 10 min reaction as a function of GO-Fe concentration. (d) The absorbance at 420 nm of pyrogallol after 1 min reaction as a function of GO-Fe concentration.

efficiency with increasing reaction time. Compared to other nanomaterials as peroxidase-like catalysts, such as Fe_3O_4 nanoparticles, the peroxidase-like color reactions were slowed down with increasing reaction time.[20] It was suggested that Fe^{2+} ions on the surface of Fe_3O_4 nanoparticles played a dominant role in the peroxidase-like activity, in which Fe^{2+} ions can react with H_2O_2 to generate the active radicals (such as •OH) and accumulate Fe^{3+} ions. However, the reaction rate of Fe^{3+} to

DOI: 10.1021/acsami.5b03486
ACS Appl. Mater. Interfaces 2015, 7, 15403−15413

Fe^{2+} ions by reacting with H_2O_2 was relatively slow in dark, leading to decreased activity of Fe_3O_4 nanoparticles. Therefore, one plausible explanation for the aforementioned peroxidase-like catalytic features of GO-Fe is the high chemical stability of GO-Fe and its accessible active sites of iron catalytic centers, which are far less limited by the diffusion and adsorption of various substances on the GO-Fe surface. Indeed, the peroxidase-like catalytic reaction on GO-Fe is performed via a nonradical pathway. Different from radical mechanism, high-valent oxo-iron species have been spectroscopically identified as active intermediates in the catalytic cycles of a number of enzymatic systems.[53] Like peroxidase and hemin, H_2O_2 can act as an oxygen-atom source to react directly with the Fe(III) state in GO-Fe, constantly generating the active oxidant (no reductant components are required in the case).

Similar to many biomimic catalytic systems,[20−27] the peroxidase-like activity of GO-Fe is dependent on pH, temperature, and H_2O_2 concentration. It is found that the catalytic activity of GO-Fe is increased as pH is decreased (Figure S9). Compared to natural peroxidase and other peroxidase-like catalysts (such as Fe_3O_4 nanoparticles), no inhibition effect on the peroxidase-like activity of GO-Fe is observed by increasing reaction temperature (Figure S10). Between 25 and 40 °C, it is revealed that $\ln\nu$ is linear with 1/K, and the activation energy of TMB color reactions in GO-Fe/H_2O_2 system is about 54 kJ/mol.

Figure 10 shows the peroxidase-like activity of GO-Fe as a function of H_2O_2 concentration. It can be seen that GO-Fe and

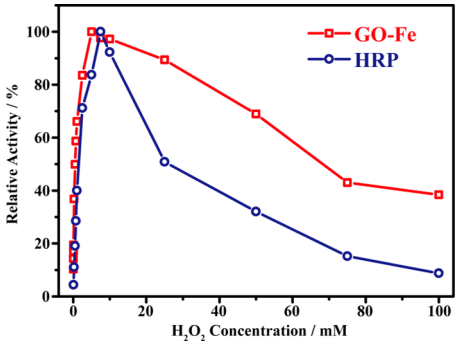

Figure 10. Dependency of peroxidase-like activity of GO-Fe and HRP with TMB as a substrate on H_2O_2 concentration, and the maximum point in each curve is set as 100%.

HRP exhibit similar profiles of activity-H_2O_2 concentration dependent curve, and the maximum points are 5 and 7.5 mM H_2O_2, respectively. Notably, GO-Fe is obviously distinct from other peroxidase-like catalysts that require a higher H_2O_2 concentration to reach the maximal level of the peroxidase-like activity. For example, Fe_3O_4 and Co_3O_4 nanoparticles need 0.53 and 2 M H_2O_2 to reach the maximum point, respectively.[20,23]

The peroxidase-like catalytic activity of GO-Fe was further investigated by studying the Michaelis−Menten behavior of TMB and pyrogallol oxidation reaction and comparing with that of HRP and hemin. Kinetic parameters for various peroxidase substrates oxidation reaction catalyzed by different catalysts are calculated according to the Michaelis−Menten equation:

$$\nu = V_{max} \times [S]/(K_m + [S])$$

where ν is the velocity under different experimental conditions, V_{max} is the maximal reaction velocity, [S] is the concentration of various substrates, and K_m is the Michaelis constant. On the basis of the different catalytic rates with varied substrate concentration, a Lineweaver−Burk plot is obtained with a linear relationship (Figures 11 and S11−S13). Furthermore, the

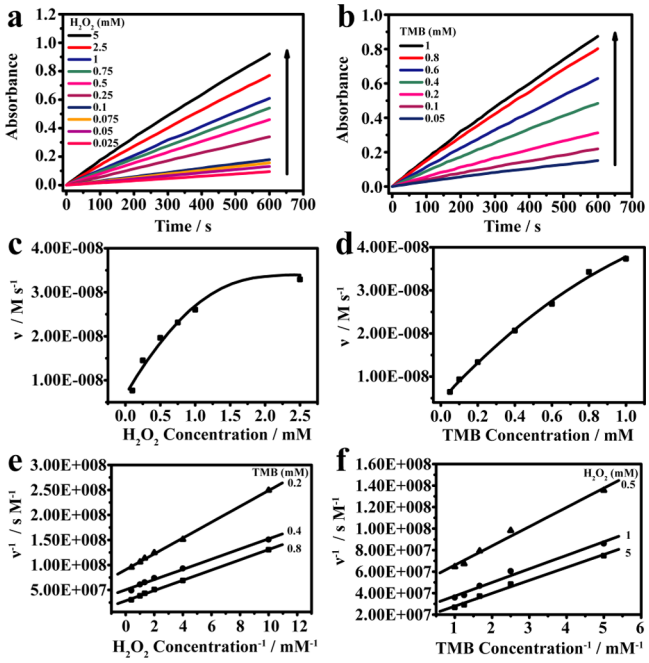

Figure 11. Time-dependent absorbance changes at 652 nm of TMB catalyzed by 2 mg/L GO-Fe at different (a) H_2O_2 and (b) TMB concentrations. (c−f) Steady-state kinetic assay and catalytic mechanism of GO-Fe with TMB as a substrate. (c, d) The reaction velocity (ν) was measured by using 2 mg/L GO-Fe at room temperature, pH 3.5. (c) The TMB concentration was 0.8 mM, and the H_2O_2 concentration was varied. (d) The H_2O_2 concentration was 5 mM, and the TMB concentration was varied. (e, f) Double-reciprocal plots of activity of GO-Fe at a fixed concentration of one substrate versus varying concentration of the second substrate for H_2O_2 and TMB.

important kinetic parameters such as K_m and k_{cat} can be derived and are given in Table S1. K_m is an expression of the substrate concentration required for the occurrence of effective catalysis, which is often associated with the affinity of the catalyst centers for the substrate. k_{cat} value reflects the maximum number of substrate molecules turned over per catalyst center per unit time under optimal conditions and can also be viewed as the optimum turnover rate. In this way, k_{cat}/K_m gives a measure of the catalytic efficiency.

The derived K_m values of GO-Fe, HRP, and hemin with H_2O_2 are 0.36, 4.98, and 1.37 mM, respectively. It is revealed that the apparent K_m value of GO-Fe with H_2O_2 is lower than that of HRP and hemin and significantly lower than that of other peroxidase-like catalysts, such as Fe_3O_4 nanoparticles (154 mM),[20] indicating that GO-Fe has higher affinity for H_2O_2. In addition, the derived K_m values of GO-Fe with peroxidase substrates TMB and pyrogallol are 0.76 and 1.93 mM, respectively, and higher than that of hemin (0.039 and 0.90 mM). In spite of weak affinity of GO-Fe for peroxidase substrates compared to hemin, the peroxidase-like catalytic activity of GO-Fe is comparable to that of hemin. For example, the derived k_{cat} values of GO-Fe are 1.3 min^{-1} for TMB and 4.6

DOI: 10.1021/acsami.5b03486
ACS Appl. Mater. Interfaces 2015, 7, 15403−15413

min^{-1} for pyrogallol, which are higher than that of hemin. The derived k_{cat} values of hemin are 0.4 min^{-1} for TMB and 2.6 min^{-1} for pyrogallol. The catalytic efficiency (k_{cat}/K_m) of GO-Fe (1680 M^{-1} min^{-1} for TMB and 2383 M^{-1} min^{-1} for pyrogallol) is also close to that of hemin (10256 M^{-1} min^{-1} for TMB and 2867 M^{-1} min^{-1} for pyrogallol). Together, these studies clearly demonstrate that iron impurities significantly enhance the catalytic performance of GO, which is close to that of the iron porphyrin systems. Hence, the important role of iron impurities in the peroxidase-like activity of graphene and its derivatives can no longer be neglected.

Since the catalytic activity of peroxidase mimics is H_2O_2-concentration-dependent, this is often used to detect H_2O_2. Furthermore, the peroxidase-like activity can be extended for the detection of glucose by coupling the above catalytic reaction with glucose oxidation reaction using glucose oxidase. The glucose oxidase oxidizes glucose and transforms O_2 into H_2O_2 quantitatively. Then, the amount of glucose can be determined indirectly according to the generated H_2O_2 taking advantage of peroxidase mimics. Figure 12 shows typical H_2O_2

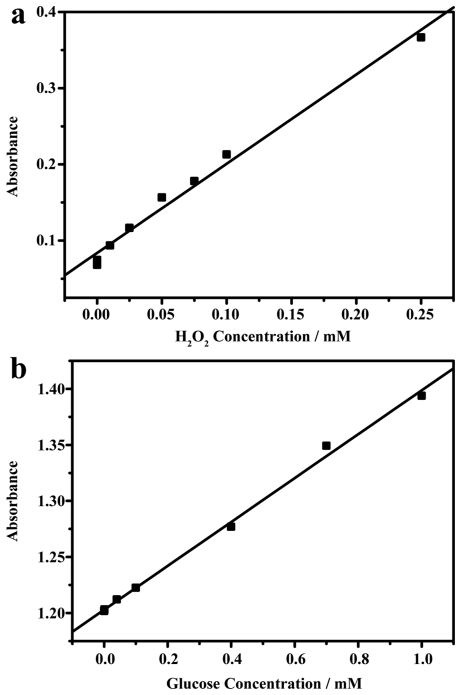

Figure 12. Linear calibration plot for (a) H_2O_2 and (b) glucose. Glucose detection was performed by the combination of GO-Fe and glucose oxidase.

and glucose concentration−response curves using GO-Fe as a peroxidase mimic for catalytic oxidation of TMB. The detection limit of H_2O_2 and glucose with various peroxidase mimics is listed in Table S2. It is demonstrated that H_2O_2 can be detected with GO-Fe as low as 1×10^{-8} M, and the linear range is from 1×10^{-7}–2.5×10^{-4} M. By using the methodology of combining the peroxidase-like catalytic reaction on GO-Fe with glucose oxidase, the lower limit and upper limit of glucose detection are 1×10^{-6} and 1×10^{-3} M, respectively. The detection ranges of both H_2O_2 and glucose are up to three orders of magnitude, being superior to most of other peroxidase mimics.

4. CONCLUSION

In summary, we have demonstrated the peroxidase-like activity of defect-free graphene, low-oxygen graphene, and iron-doped GO as well as GO. Iron impurities could inherently exist in graphene and its derivatives, and very likely act as active sites for the peroxidase-like catalytic reaction instead of the intrinsic features, such as the active oxygen moieties for GO and the structural defects for high quality graphene. According to our findings, it is highly recommended to roundly assess the features of active sites in the peroxidase-like catalytic reaction on all nonmetallic materials, especially carbon nanomaterials. Only in this way can we determinately declare that the nonmetallic materials possess "intrinsic or metal-free peroxidase-like activity". Note that other features of materials, such as the dispersibility in reaction medium, have profound influences on the observed catalytic activity and our further judgements concerning the nature of active sites.

Everything has two sides. On one hand, metallic impurities dramatically change the intrinsic features of carbon nanomaterials such as electronic, electrochemical, redox, catalytic, and toxicological properties. On the other hand, we can utilize the non-negligible impact of metallic impurities on the properties of carbon nanomaterials to extend their applications. For example, here we have immobilized saturated iron(III) onto the oxygen-donor coordination of GO to enhance its peroxidase-like activity for the highest possible. This iron(III) doped GO has been successfully used to quantitatively detect H_2O_2 and glucose. Furthermore, future work will focus on adjusting the structures of graphene derivatives and commanding the interaction between metallic impurities and various functional groups of graphene derivatives to improve the performances and expand the applications of graphene-based materials.

■ ASSOCIATED CONTENT

Supporting Information

SEM, TEM, XPS of defect-free graphene; UV−vis absorption spectrum of TMB oxidization catalyzed by defect-free graphene; XPS, TGA, AFM of GO-Fe; the effect of pH and temperature on the peroxidase-like activity of GO-Fe; kinetic studies on the peroxidase-like activity of GO-Fe, HRP, and hemin. The Supporting Information is available free of charge on the ACS Publications website at DOI: 10.1021/acsami.5b03486.

■ AUTHOR INFORMATION

Corresponding Authors

*E-mail: jli@licp.cas.cn.
*E-mail: zguo@licp.cas.cn.

Notes

The authors declare no competing financial interest.

■ ACKNOWLEDGMENTS

This work was supported by the National Nature Science Foundation of China (Nos. 21203217 and 11172301) and the "Top Hundred Talents" Program of Chinese Academy of Sciences.

■ REFERENCES

(1) Lombardi, A.; Nastri, F.; Pavone, V. Peptide-Based Heme−Protein Models. *Chem. Rev.* **2001**, *101*, 3165−3189.

DOI: 10.1021/acsami.5b03486
ACS Appl. Mater. Interfaces 2015, 7, 15403−15413

(2) Yamaguchi, H.; Tsubouchi, K.; Kawaguchi, K.; Horita, E.; Harada, A. Peroxidase Activity of Cationic Metalloporphyrin-Antibody Complexes. *Chem. - Eur. J.* **2004**, *10*, 6179−6186.
(3) Shema-Mizrachi, M.; Pavan, G. M.; Levin, E.; Danani, A.; Lemcoff, N. G. Catalytic Chameleon Dendrimers. *J. Am. Chem. Soc.* **2011**, *133*, 14359−14367.
(4) Astruc, D. Electron-Transfer Processes in Dendrimers and Their Implication in Biology, Catalysis, Sensing and Nanotechnology. *Nat. Chem.* **2012**, *4*, 255−267.
(5) Wang, Q.; Yang, Z.; Zhang, X.; Xiao, X.; Chang, C. K.; Xu, B. A Supramolecular-Hydrogel-Encapsulated Hemin as an Artificial Enzyme to Mimic Peroxidase. *Angew. Chem., Int. Ed.* **2007**, *46*, 4285−4289.
(6) Ishida, Y.; Shimada, T.; Masui, D.; Tachibana, H.; Inoue, H.; Takagi, S. Efficient Excited Energy Transfer Reaction in Clay Porphyrin Complex toward an Artificial Light-Harvesting System. *J. Am. Chem. Soc.* **2011**, *133*, 14280−14286.
(7) Fateeva, A.; Devautour-Vinot, S.; Heymans, N.; Devic, T.; Grenèche, J.-M.; Wuttke, S.; Miller, S.; Lago, A.; Serre, C.; De Weireld, G.; Maurin, G.; Vimont, A.; Férey, G. Series of Porous 3-D Coordination Polymers Based on Iron(III) and Porphyrin Derivatives. *Chem. Mater.* **2011**, *23*, 4641−4651.
(8) Kato, M.; Cardona, T.; Rutherford, A. W.; Reisner, E. Photoelectrochemical Water Oxidation with Photosystem II Integrated in a Mesoporous Indium−Tin Oxide Electrode. *J. Am. Chem. Soc.* **2012**, *134*, 8332−8335.
(9) Conklin, D.; Nanayakkara, S.; Park, T.-H.; Lagadec, M. F.; Stecher, J. T.; Therien, M. J.; Bonnell, D. A. Electronic Transport in Porphyrin Supermolecule-Gold Nanoparticle Assemblies. *Nano Lett.* **2012**, *12*, 2414−2419.
(10) Novoselov, K. S.; Geim, A. K.; Morozov, S. V.; Jiang, D.; Zhang, Y.; Dubonos, S. V.; Grigorieva, I. V.; Firsov, A. A. Electric Field Effect in Atomically Thin Carbon Films. *Science* **2004**, *306*, 666−669.
(11) Balandin, A. A.; Ghosh, S.; Bao, W.; Calizo, I.; Teweldebrhan, D.; Miao, F.; Lau, C. N. Superior Thermal Conductivity of Single-Layer Graphene. *Nano Lett.* **2008**, *8*, 902−907.
(12) Lee, C.; Wei, X.; Kysar, J. W.; Hone, J. Measurement of the Elastic Properties and Intrinsic Strength of Monolayer Graphene. *Science* **2008**, *321*, 385−388.
(13) Bolotin, K. I.; Sikes, K. J.; Jiang, Z.; Klima, M.; Fudenberg, G.; Hone, J.; Kim, P.; Stormer, H. L. Ultrahigh Electron Mobility in Suspended Graphene. *Solid State Commun.* **2008**, *146*, 351−355.
(14) Stoller, M. D.; Park, S.; Zhu, Y.; An, J.; Ruoff, R. S. Graphene-Based Ultracapacitors. *Nano Lett.* **2008**, *8*, 3498−3502.
(15) Huang, C.; Bai, H.; Li, C.; Shi, G. A Graphene Oxide Hemoglobin Composite Hydrogel for Enzymatic Catalysis in Organic Solvents. *Chem. Commun.* **2011**, *47*, 4962−4964.
(16) Xue, T.; Jiang, S.; Qu, Y.; Su, Q.; Cheng, R.; Dubin, S.; Chiu, C.-Y.; Kaner, R.; Huang, Y.; Duan, X. Graphene-Supported Hemin as a Highly Active Biomimetic Oxidation Catalyst. *Angew. Chem., Int. Ed.* **2012**, *51*, 3822−3825.
(17) Wang, Q.; Lei, J.; Deng, S.; Zhang, L.; Ju, H. Graphene-Supported Ferric Porphyrin as a Peroxidase Mimic for Electrochemical DNA Biosensing. *Chem. Commun.* **2013**, *49*, 916−918.
(18) Lu, L.-M.; Qiu, X.-L.; Zhang, X.-B.; Shen, G.-L.; Tan, W.; Yu, R.-Q. Supramolecular Assembly of Enzyme on Functionalized Graphene for Electrochemical Biosensing. *Biosens. Bioelectron.* **2013**, *45*, 102−107.
(19) Zhang, L.; Han, G.; Liu, Y.; Tang, J.; Tang, W. Immobilizing Haemoglobin on Gold Graphene−Chitosan Nanocomposite as Efficient Hydrogen Peroxide Biosensor. *Sens. Actuators, B* **2014**, *197*, 164−171.
(20) Gao, L.; Zhuang, J.; Nie, L.; Zhang, J.; Zhang, Y.; Gu, N.; Wang, T.; Feng, J.; Yang, D.; Perrett, S.; Yan, X. Intrinsic Peroxidase-Like Activity of Ferromagnetic Nanoparticles. *Nat. Nanotechnol.* **2007**, *2*, 577−583.
(21) Jv, Y.; Li, B.; Cao, R. Positively-Charged Gold Nanoparticles as Peroxidiase Mimic and Their Application in Hydrogen Peroxide and Glucose Detection. *Chem. Commun.* **2010**, *46*, 8017−8019.
(22) Wang, X.-X.; Wu, Q.; Shan, Z.; Huang, Q.-M. BSA-Stabilized Au Clusters as Peroxidase Mimetics for Use in Xanthine Detection. *Biosens. Bioelectron.* **2011**, *26*, 3614−3619.
(23) Mu, J.; Wang, Y.; Zhao, M.; Zhang, L. Intrinsic Peroxidase-Like Activity and Catalase-Like Activity of Co_3O_4 Nanoparticles. *Chem. Commun.* **2012**, *48*, 2540−2542.
(24) Dong, Y.; Zhang, H.; Rahman, Z. U.; Su, L.; Chen, X.; Hu, J.; Chen, X. Graphene Oxide-Fe_3O_4 Magnetic Nanocomposites with Peroxidase-Like Activity for Colorimetric Detection of Glucose. *Nanoscale* **2012**, *4*, 3969−3976.
(25) Liu, M.; Zhao, H.; Chen, S.; Yu, H.; Quan, X. Interface Engineering Catalytic Graphene for Smart Colorimetric Biosensing. *ACS Nano* **2012**, *6*, 3142−3151.
(26) Zhang, Z.; Hao, J.; Yang, W.; Lu, B.; Ke, X.; Zhang, B.; Tang, J. Porous Co_3O_4 Nanorods−Reduced Graphene Oxide with Intrinsic Peroxidase-Like Activity and Catalysis in the Degradation of Methylene Blue. *ACS Appl. Mater. Interfaces* **2013**, *5*, 3809−3815.
(27) Tao, Y.; Lin, Y.; Huang, Z.; Ren, J.; Qu, X. Incorporating Graphene Oxide and Gold Nanoclusters: A Synergistic Catalyst with Surprisingly High Peroxidase-Like Activity Over a Broad pH Range and its Application for Cancer Cell Detection. *Adv. Mater.* **2013**, *25*, 2594−2599.
(28) Song, Y.; Qu, K.; Zhao, C.; Ren, J.; Qu, X. Graphene Oxide Intrinsic Peroxidase Catalytic Activity and Its Application to Glucose Detection. *Adv. Mater.* **2010**, *22*, 2206−2210.
(29) Wang, Y.; Shao, Y.; Matson, D. W.; Li, J.; Lin, Y. Nitrogen-Doped Graphene and Its Application in Electrochemical Biosensing. *ACS Nano* **2010**, *4*, 1790−1798.
(30) Song, Y.; Wang, X.; Zhao, C.; Qu, K.; Ren, J.; Qu, X. Label-Free Colorimetric Detection of Single Nucleotide Polymorphism by Using Single-Walled Carbon Nanotube Intrinsic Peroxidase-Like Activity. *Chem. - Eur. J.* **2010**, *16*, 3617−3621.
(31) Shi, W.; Wang, Q.; Long, Y.; Cheng, Z.; Chen, S.; Zheng, H.; Huang, Y. Carbon Nanodots as Peroxidase Mimetics and Their Applications to Glucose Detection. *Chem. Commun.* **2011**, *47*, 6695−6697.
(32) Cui, R.; Han, Z.; Zhu, J.-J. Helical Carbon Nanotubes Intrinsic Peroxidase Catalytic Activity and Its Application for Biocatalysis and Biosensing. *Chem. - Eur. J.* **2011**, *17*, 9377−9384.
(33) Wang, X.; Jiao, L.; Sheng, K.; Li, C.; Dai, L.; Shi, G. Solution-Processable Graphene Nanomeshes with Controlled Pore Structures. *Sci. Rep.* **2012**, *3*, 1996−2000.
(34) Šljukić, B.; Banks, C. E.; Compton, R. G. Iron Oxide Particles Are The Active Sites for Hydrogen Peroxide Sensing at Multiwalled Carbon Nanotube Modified Electrodes. *Nano Lett.* **2006**, *6*, 1556−1558.
(35) Ambrosi, A.; Chua, C. K.; Khezri, B.; Sofer, Z.; Webster, R. D.; Pumera, M. Chemically Reduced Graphene Contains Inherent Metallic Impurities Present in Parent Natural and Synthetic Graphite. *Proc. Natl. Acad. Sci. U. S. A.* **2012**, *109*, 12899−12904.
(36) Pumera, M.; Ambrosi, A.; Chng, E. L. K. Impurities in Graphenes and Carbon Nanotubes and Their Influence on the Redox Properties. *Chem. Sci.* **2012**, *3*, 3347−3355.
(37) Wang, L.; Ambrosi, A.; Pumera, M. "Metal-Free" Catalytic Oxygen Reduction Reaction on Heteroatom-Doped Graphene is Caused by Trace Metal Impurities. *Angew. Chem., Int. Ed.* **2013**, *52*, 13818−13821.
(38) Dreyer, D. R.; Jia, H.-P.; Bielawski, C. W. Graphene Oxide: A Convenient Carbocatalyst for Facilitating Oxidation and Hydration Reactions. *Angew. Chem., Int. Ed.* **2010**, *49*, 6813−6816.
(39) Dreyer, D. R.; Bielawski, C. W. Carbocatalysis: Heterogeneous Carbons Finding Utility in Synthetic Chemistry. *Chem. Sci.* **2011**, *2*, 1233−1240.
(40) Su, C.; Acik, M.; Takai, K.; Lu, J.; Hao, S.; Zheng, Y.; Wu, P.; Bao, Q.; Enoki, T.; Chabal, Y. J.; Ping Loh, K. Probing the Catalytic Activity of Porous Graphene Oxide and the Origin of This Behavior. *Nat. Commun.* **2012**, *3*, 1298−1306.
(41) Hernandez, Y.; Nicolosi, V.; Lotya, M.; Blighe, F. M.; Sun, Z. Y.; De, S.; McGovern, I. T.; Holland, B.; Byrne, M.; Gun'ko, Y. K.;

DOI: 10.1021/acsami.5b03486
ACS Appl. Mater. Interfaces 2015, 7, 15403−15413

Boland, J. J.; Niraj, P.; Duesberg, G.; Krishnamurthy, S.; Goodhue, R.; Hutchison, J.; Scardaci, V.; Ferrari, A. C.; Coleman, J. N. High-Yield Production of Graphene by Liquid-Phase Exfoliation of Graphite. *Nat. Nanotechnol.* **2008**, *3*, 563−568.
(42) Khan, U.; O'Neill, A.; Lotya, M.; De, S.; Coleman, J. N. High-Concentration Solvent Exfoliation of Graphene. *Small* **2010**, *6*, 864−871.
(43) Dong, Y.; Li, J.; Shi, L.; Wang, X.; Guo, Z.; Liu, W. Significant Advantages of Low-Oxygen Graphene Nanosheets. *J. Mater. Chem. A* **2015**, *3*, 9738−9744.
(44) Hummers, W. S.; Offeman, R. E. Preparation of Graphitic Oxide. *J. Am. Chem. Soc.* **1958**, *80*, 1339.
(45) Dong, Y.; Li, J.; Shi, L.; Xu, J.; Wang, X.; Guo, Z.; Liu, W. Graphene Oxide−Iron Complex: Synthesis, Characterization and Visible-Light-Driven Photocatalysis. *J. Mater. Chem. A* **2013**, *1*, 644−650.
(46) Dreyer, D. R.; Park, S.; Bielawski, C. W.; Ruoff, R. S. The Chemistry of Graphene Oxide. *Chem. Soc. Rev.* **2010**, *39*, 228−240.
(47) Bai, H.; Li, C.; Wang, X.; Shi, G. On the Gelation of Graphene Oxide. *J. Phys. Chem. C* **2011**, *115*, 5545−5551.
(48) Cong, H.-P.; Ren, X.-C.; Wang, P.; Yu, S.-H. Macroscopic Multifunctional Graphene-Based Hydrogels and Aerogels by a Metal Ion Induced Self-Assembly Process. *ACS Nano* **2012**, *6*, 2693−2703.
(49) Shih, C.-J.; Lin, S.; Strano, M. S.; Blankschtein, D. Understanding the Stabilization of Liquid-Phase-Exfoliated Graphene in Polar Solvents Molecular Dynamics Simulations and Kinetic Theory of Colloid Aggregation. *J. Am. Chem. Soc.* **2010**, *132*, 14638−14648.
(50) Keeley, G. P.; O'Neill, A.; McEvoy, N.; Peltekis, N.; Coleman, J. N.; Duesberg, G. S. Electrochemical Ascorbic Acid Sensor Based on DMF-Exfoliated Graphene. *J. Mater. Chem.* **2010**, *20*, 7864−7869.
(51) Qi, S.; Zhao, B.; Tang, H.; Jiang, X. Determination of Ascorbic Acid, Dopamine, and Uric Acid by a Novel Electrochemical Sensor Based on Pristine Graphene. *Electrochim. Acta* **2015**, *161*, 395−402.
(52) Wu, C.; Cheng, Q.; Wu, K. Electrochemical Functionalization of N-Methyl-2-pyrrolidone-Exfoliated Graphene Nanosheets as Highly Sensitive Analytical Platform for Phenols. *Anal. Chem.* **2015**, *87*, 3294−3299.
(53) Hohenberger, J.; Ray, K.; Meyer, K. The Biology and Chemistry of High-Valent Iron−Oxo and Iron−Nitrido Complexes. *Nat. Commun.* **2012**, *3*, 720−732.

DOI: 10.1021/acsami.5b03486
ACS Appl. Mater. Interfaces 2015, 7, 15403−15413